Membrane shape as a reporter for applied forces

Heun Jin Lee[a], Eric L. Peterson[a], Rob Phillips[a], William S. Klug[b], and Paul A. Wiggins[c,1]

[a]Departments of Applied Physics, Biochemistry and Molecular Biophysics, and Mechanical Engineering, California Institute of Technology, 1200 East California Boulevard, Pasadena, CA 91125; [b]Department of Mechanical and Aerospace Engineering and Program in Biomedical Engineering, University of California, Los Angeles, CA 90095; and [c]Whitehead Institute for Biomedical Research, 9 Cambridge Center, Cambridge, MA 02142

Edited by L. B. Freund, Brown University, Providence, RI, and approved October 22, 2008 (received for review July 15, 2008)

Recent advances have enabled 3-dimensional reconstructions of biological structures in vivo, ranging in size and complexity from single proteins to multicellular structures. In particular, tomography and confocal microscopy have been exploited to capture detailed 3-dimensional conformations of membranes in cellular processes ranging from viral budding and organelle maintenance to phagocytosis. Despite the wealth of membrane structures available, there is as yet no generic, quantitative method for their interpretation. We propose that by modeling these observed biomembrane shapes as fluid lipid bilayers in mechanical equilibrium, the externally applied forces as well as the pressure, tension, and spontaneous curvature can be computed directly from the shape alone. To illustrate the potential power of this technique, we apply an axial force with optical tweezers to vesicles and explicitly demonstrate that the applied force is equal to the force computed from the membrane conformation.

lipid bilayers | membrane mechanics | optical trapping | membrane tethering

Biomembranes, phospholipid bilayers that form the boundaries of cells and compartmentalize cellular organelles, are intricately and dynamically structured on the submicrometer length scale (1). The cellular membrane must undergo constant conformational remodeling in diverse cellular processes, ranging from intracellular trafficking (vesiculation and endocytosis) to the biogenesis of membrane-bound organelles. These intricate structures are precisely regulated and are integral to organelle and cellular function (1). Recent advances in microscopy have resulted in an increasingly detailed structural picture of cellular membranes and organelles. For instance, cryoelectron tomography has enabled the reconstruction of high-resolution, 3-dimensional models of organelle structure [the mitochondrion (2), the Golgi apparatus (3), and the endoplasmic reticulum (3)] as well as HIV viral entry (4), and the endocytotic machinery (5). Similarly, confocal and "super-resolution" fluorescence microscopy have emerged as a powerful tool for the capture of 3-dimensional cellular structure (6–8).

Although these microscopy-based membrane structures have led to revolutions in our qualitative understanding of membrane morphology, no general technique exists as yet for their quantitative analysis. In particular, a number of mechanisms have been identified that deform the membrane (1): the aggregation of transmembrane proteins (9, 10), active remodeling by molecular motors (11–13), assembly and disassembly of cytoskeletal filaments (14–16), and direct or indirect scaffolding by proteins (17, 18). However, the study of these mechanisms has been limited, especially in vivo. For instance, it has long been postulated that the mechanics of the membrane plays an important role in the aggregation of membrane proteins (19), and recent simulations have also lent support to this idea (20). In this case, knowledge of the mechanical forces applied by aggregating membrane proteins to an experimentally observed membrane structure would shed further light on their size, distribution, and mutual interaction. The quantitative measurement of the location and magnitude of the forces applied by cellular machinery promises to yield important insights into the detailed mechanisms of membrane-remodeling processes, from the life cycle of a membrane-bound virus to the scaffolding underlying organelle structure.

In this article, (*i*) we propose a quantitative technique for computing the external forces applied to a membrane from the observed membrane conformation; (*ii*) we apply this method to explicitly demonstrate that conformation-based force computation agrees with the applied force in an optical-tweezer-driven membrane-tether-pulling experiment. The conformation-based method of force measurement that we describe here represents a meeting of theoretical, computational, and experimental approaches, demonstrating that the Helfrich–Canham–Evans theory of lipid bilayers allows measurement of mechanical force from an observed membrane conformation in a subpiconewton optical tweezing experiment. Finally, (*iii*) we argue that the symmetric, 2-dimensional implementation demonstrated here may be extended with specialized state-of-the-art finite-element methods (21) to calculate the forces applied to arbitrary membrane shapes measured via electron tomography or fluorescence microscopy. We argue that these techniques may be extended to describe the forces shaping in vivo biomembranes, although the interpretation of these structures is complicated by the heterogeneity of the biomembranes themselves (22).

Results

The mechanical theory of fluid-phase lipid membranes has been the subject of extensive study (22, 23) and experiments suggest that the response of membranes to the application of force is well-approximated by the theory of Helfrich, Canham, and Evans (24–26). The Helfrich model describes the conformational energy of the membrane in terms of an energy density ε that is a function of the local shape of the membrane:

$$\varepsilon = \tfrac{1}{2} k_C (S^2 - 2CS). \qquad [1]$$

where S is the sum of the principal curvatures with associated bending modulus k_C and C is the spontaneous curvature. The spontaneous curvature describes the spontaneous bending of the membrane induced by asymmetries in the lipid composition or chemical environment of the individual leaflets. The elastic force density applied by the membrane is determined by performing the first variation of the Helfrich energy (27). Because the membrane is fluid in-plane (28, 29), the equilibrium elastic force per unit area is in the direction perpendicular to the membrane:

$$f_\perp = S\alpha - p - k_C [\nabla^2 S - 2K (S - C) + \tfrac{1}{2} S^3], \qquad [2]$$

Author contributions: H.J.L., E.L.P., R.P., and P.A.W. designed research; H.J.L., E.L.P., and P.A.W. performed research; H.J.L., E.L.P., W.S.K., and P.A.W. analyzed data; and H.J.L., E.L.P., R.P., W.S.K., and P.A.W. wrote the paper.

The authors declare no conflict of interest.

This article is a PNAS Direct Submission.

[1]To whom correspondence should be addressed. E-mail: wiggins@wi.mit.edu.

This article contains supporting information online at www.pnas.org/cgi/content/full/0806814105/DCSupplemental.

where K is the Gaussian curvature (the product of the principal curvatures); the parameters α and p are the tension and pressure difference over the membrane, respectively. In equilibrium, this force density is zero. Note that when the bending modulus is zero, this equation reduces to the Young–Laplace equation for soap films. The local force density depends on the local membrane geometry, which is directly observable, and 3 Lagrange multipliers, the pressure, tension, and spontaneous curvature, which must be determined. To compute these unknown Lagrange multipliers, we apply the *Proximal Equilibrium Approximation* that uses a maximum-likelihood principle to determine the values of pressure, tension, and spontaneous curvature which predict an equilibrium conformation closest to the observed conformation. [The Proximal Equilibrium Approximation is described in more detail in the supporting information (SI) *Appendix*.]

The total elastic force applied by a region of the membrane is calculated as the integral over the force density in that region. Because the stress tensor can also be written as a function of the membrane geometry and the Lagrange multipliers, the total elastic force (applied by the membrane) can be computed as a contour integral on the region boundary (30). (See the *SI Appendix* for an explanation of this technique and additional references.) Evaluating the force at the boundary has 2 significant practical advantages over the direct integration of the predicted force density: (*i*) the boundary integral depends on lower-order numerical derivatives, making it less sensitive to experimental noise, and (*ii*) regions of the membrane where the structure is poorly determined can be bypassed. We term the force measured in this way from the membrane morphology the "conformational force," because it is based purely on information contained in the observed shape of the membrane.

Force-induced membrane tether formation (31, 32) provides a convenient test of the conformational force computation: a known force, applied to an optically trapped bead, can be directly compared with the conformational force. The progression of vesicle shapes in our experiment as the tether forms is illustrated by the membrane conformations shown in gray in the background of Fig. 3. As the axial force is increased, the vesicle first assumes an elongated shape before reaching a transition in which a cylindrical tether forms at 1 end of the vesicle. This transition is seen in reverse in the retraction phase of the experiment. In our experiment, forces were applied via optically trapped beads to DOPC giant unilamellar vesicles. The streptavidin-coated beads were linked to the vesicles via biotin-labeled lipids. The bending modulus k_C for DOPC is 0.85×10^{-19} J (33). The structure of the vesicles in these experiments is captured via fluorescence microscopy and is limited in 2 respects: (*i*) the observed membrane shape is based on imaging the midplane of the vesicle and axial symmetry must be assumed to construct the 3-dimensional structure, and (*ii*) the resolution of the membrane structures is the optical-diffraction limit.

In a typical experiment, 50 fluorescent images were captured at each step in an extension series. (All of the structures for the dataset discussed in the text are shown in the *SI Appendix*.) An extension series typically consisted of between 50 and 60 steps split between extension and retraction, with a step size of $\approx$1.5 μm. The integration time was chosen to give sufficient pixel statistics to allow the contour of the membrane in each image to be traced independently. The vesicle conformation is represented as a cubic spline with control vertices as shown in Fig. 1. The position of the vertices in the direction parallel to membrane surface was chosen by hand; the position in the direction perpendicular to the surface was fit to the fluorescence profile independently in each frame. [The capture of the instantaneous structure allows the comparison of the thermal undulations with the predicted stiffness matrix (H.J.L., E.L.P., and P.A.W., unpublished data).] In our analysis, we will assume that the vesicle is axially symmetric so that the observed cross-sectional structure determines the entire vesicle structure. This approximation is excellent at large extensions, but breaks down at low force.

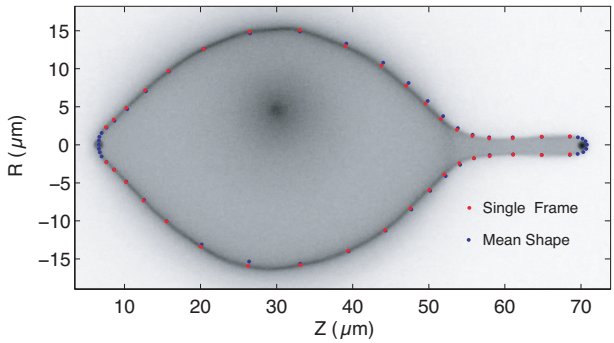

Fig. 1. Capturing the membrane conformation. A fluorescence image of a vesicle from a force-extension series. The vesicle conformation is represented as a cubic spline. The positions of the control vertices are fit from the fluorescence profile. The red vertices were traced from the fluorescence image shown in the figure; the blue vertices correspond to a trace of the mean of the 50 images at this extension. The deviation of the instantaneous structure (red) from the mean structure (blue) is a consequence of the long-wavelength thermal undulations.

A typical single fluorescence image of a tethered vesicle is shown in Fig. 1 together with the vertices traced from the image frame. The mechanics of the membrane should be independent of a particular vertex representation: observable physical quantities cannot depend on the positions of the control vertices in the direction parallel to the membrane surface. The individual vertex forces f_i do depend on the vertex position for 2 reasons: the vertex positions control the effective area of each vertex, and the vertex force depends on the 4th derivative of the vertex positions and is therefore susceptible to noise. However, the equilibrium displacement ψ_i, the estimated displacement to the equilibrium conformation at each vertex, is approximately independent of the effective vertex area and suppresses the derivative noise because high-frequency modes have a high stiffness* (see Fig. 2*A*). To implement the Proximal Equilibrium Approximation, we therefore minimized the square of the equilibrium displacements at each vertex to determine the Lagrange multipliers. Fig. 2*A* shows that the measured conformation closely matches the estimated equilibrium conformation for the optimized Lagrange multipliers (pressure, 3.4 ± 0.2 mPa; tension, $7.4 \pm 0.5\, k_BT/\mu m^2$; and spontaneous curvature, $-0.27 \pm 0.10\ \mu m^{-1}$) determined by the Proximal Equilibrium Approximation. Despite the apparent representation dependence of the vertex forces, we find that the integrated force results in consistent force predictions. In Fig. 2*B*, we plot the integrated force for slices of the vesicle perpendicular to the z axis. As expected, this force is nearly constant throughout the body of the vesicle, a key consistency condition because forces are applied only at the axial poles of the vesicle.

To demonstrate the power of conformation force computation, we explicitly show that the conformational forces correctly predict the applied force as a tether is pulled from a vesicle by an optical tweezer. To resolve the structure of tethered vesicles by light microscopy, the force at which tethers formed had to be $<$2 pN, implying that the undeformed vesicles had a large excess of area (low tension). In Fig. 3, we compare the conformational forces to the applied force for a tether extension and retraction.

*We demonstrated the representation independence by making independent tracings of each dataset, which resulted in nearly identical measurements of physically observable quantities. For more information see the *SI Appendix*.

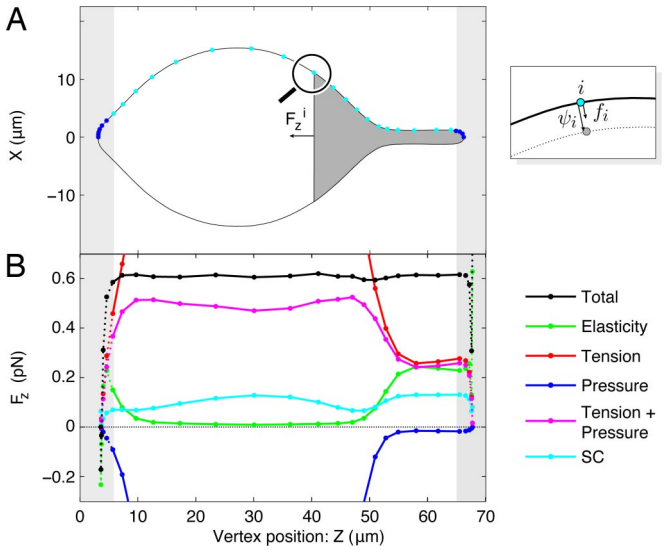

Fig. 2. The Proximal Equilibrium Approximation. (*A*) Vesicle conformation: The axisymmetric vesicle conformation is represented as a cubic spline. The control vertices are shown as points along the contour. To find the pressure, tension, and spontaneous curvature of the membrane, we choose initial values of these parameters which produce a trial membrane configuration. On the right we show a magnified view of the observed membrane shape (solid curve) as well as the trial shape (dotted line) near control vertex *i* where the displacement between the vertex in the observed shape (light blue) and the trial shape (light gray) is labeled as ψ_i. We minimize the mean-square displacements ψ_i with respect to the trial values of pressure, tension, and spontaneous curvature to form a best estimate for the values of these parameters. During the minimization we exclude the regions in the proximity of the bead attachment points, shaded in gray on the left and right, where the membrane shape cannot be resolved with sufficient precision to make reliable force estimates. (*B*) Summed force: The summed force at vertex *i*, F_z^i, is the sum of the *z* components of the vertex forces in the dark-gray region which excludes vertices with $z < z_i$. F_z^i is the total force applied by the right-hand side of the vesicle in the *z* direction. In *B* we plot the total summed force (black), which, as expected, is approximately constant throughout the body of the vesicle, because the forces are applied only at the poles of the vesicle. The summed force is also shown decomposed into individual contributions from pressure, tension, spontaneous curvature, and bending elasticity.

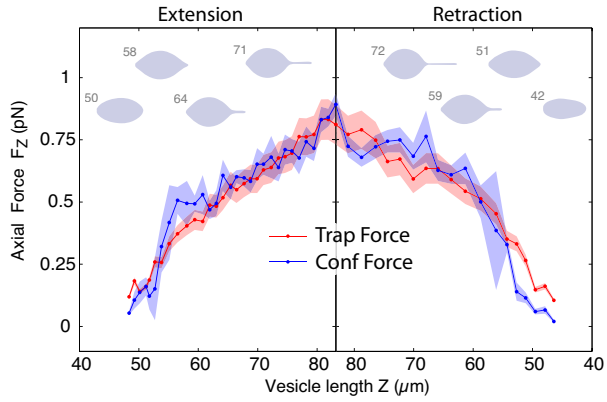

Fig. 3. Comparison of the applied and conformational force. The computed conformational force (blue curve) and the applied trapping force (red curve) are in both qualitative and quantitative agreement from 0.1 to 1 pN. The shaded regions are the error in the trapping force and the rms variation in the conformational force, respectively. Note that the *x* axis orientation has been inverted in the retraction data. (*Inset*) Membrane conformations as a function of axial length (μm).

(The corresponding optimized Lagrange multipliers are plotted in the *SI Appendix*.) We measure a mean relative error of 10% for forces in the range of 0.2 to 1 pN, showing that the applied and conformational force are in both qualitative and quantitative agreement in that range. The optical tweezing force measurements suffered from 2 important shortcomings in the subpiconewton regime: (*i*) Subpiconewton force measurements are generically susceptible to drift. (*ii*) The vesicles themselves were also found to weakly scatter the trapping beam, resulting in anomalous force signals during large-scale changes in vesicle structure. For instance, only datasets where the force sensor bead was not positioned on the end of the tether were found to result in consistent force traces. The mismatch between conformational and applied forces appears to increase toward the end of the retraction, consistent with both trap drift and membrane conformation-induced beam scattering. Our analysis also revealed limitations in the conformational force technique. For very low forces, the conformational force is limited by the determination of the Lagrange multipliers. At high force, the conformational force is limited by diffraction as the typical length scale of the neck of the tether shrinks below that limit.

Discussion

The central theme of this work is the development and validation of a framework that is *generally applicable* to the computation of mechanical forces applied to a membrane of arbitrary shape, including the contributions of pressure, tension, and spontaneous curvature. Although the formation of membrane tethers is both well-known and well-studied in the membrane mechanics literature (34–37), it nevertheless provides a convenient proof-of-principle experiment where both the force, applied by the optical trap, and the membrane conformation are known simultaneously. Similarly, a direct analysis of membrane conformation has been performed by Baumgart and coworkers to measure the material properties and line tension in multiphase vesicles (38). However, the analysis techniques described in ref. 39 are of limited applicability to the computations of forces for nonaxisymmetric conformations or tethered vesicles. [These limitations are discussed further in the *SI Appendix*. In particular, the computation of tethered-vesicle structure via direct integration is numerically problematic (36).] Although our measurements have been restricted to structures derived from light microscopy, the full potential of the conformation-based force measurement technique lies in the fully 3-dimensional structures captured via tomography or confocal microscopy. Computational techniques to analyze 3-dimensional membrane conformations have been described elsewhere (21) and would extend our framework in a natural way to general membrane structures.

Although the conformational force calculations, described in this article, could in principle be used to describe pipette aspiration experiments, this analysis would be less accurate than canonical techniques because these canonical methods parameterize the vesicle conformation with fewer parameters that can therefore be determined with higher precision. (See ref. 39, for instance.) However, we expect conformational force calculations to be a powerful tool for analyzing in vitro membrane conformation in experiments where the membrane conformation cannot be simply parameterized. The most exciting potential applications are the analysis of in vivo biomembrane-remodeling processes. We can estimate the spatial resolution required to image structures of interest by examining the dependence of the force at tether formation on curvature. [The tether-force equation is the exact equilibrium force required to support a tether radius R in the absence of spontaneous curvature (35).] Given an applied force F, the approximate scale of membrane bending R is given by $R \sim 2\pi k_C/F = 0.4\ (1\ \text{pN}/F)\ \mu\text{m}$. Because the typical protein-scale biological forces are several piconewtons, the

conformational force technique will be most powerful in the analysis of structure captured at resolutions higher than the optical diffraction limit. There are no other experimental tools that allow the measurement of forces applied to biomembranes in vivo. Previous experiments have been limited to the extrusion of tethers from living cells, but these experiments probe deformations on scales beyond those normally experienced by the cell in biomembrane-remodeling processes (40, 41).

The greatest challenge to extending these techniques to in vivo biomembranes is the heterogeneity of the biomembranes themselves. The analysis of membranes with phase boundaries adds considerable complexity to the problem (22). Despite these difficulties, the technique described here exhibits a number of powerful properties that may help to circumvent these potential pitfalls. For instance, even in a case where the biomembrane structure cannot be resolved in a localized region because of the presence of a large protein scaffold or lipid raft, we may still measure forces provided a surrounding region of fluid biomembrane exists, because the boundary force method only requires knowledge of the shape of the membrane on the *boundary* of a region of interest. This feature is also essential for the analysis of data from electron tomography which are typically incomplete because of the "missing wedge" artifact.

Another potentially daunting challenge is the determination of the Lagrange multipliers for in vivo systems where the number of contact points is potentially much greater than the tethered vesicles discussed in this article. But the determination of 3 Lagrange multipliers by using the Proximal Equilibrium Approximation is a peculiarity of the in vitro tether formation process where the membrane undergoes a dramatic conformational change on the same scale as the vesicle itself. For most biological membrane-remodeling examples, the pressure is negligibly small where the membrane mechanics is relevant. Furthermore, studies suggest that the tension (and spontaneous curvature) may be a regulated property of many cytoplasmic and organelle biomembranes (40). When the Lagrange multipliers are known or determined, the forces can be directly computed.

Despite these potential limitations, quantitative analysis of the membrane structure holds the promise of probing the forces and structural elements that are at work in biological membrane-remodeling processes that intricately shape biological membranes and are integral to organelle and cellular function. For instance, quantitative structural analysis could reveal the structural nature of the scaffolds that dynamically maintain and remodel organelle biomembranes. Are scaffolds necessary to maintain the structure of mitochondrial cristae and cristae junctions in the inner membrane? What is the structural basis for the creation and maintenance of the interconnected fenestrations in the Golgi apparatus and endoplasmic reticulum? Quantitative structural analysis could also be exploited to quantitatively test the aggregation-driven models of HIV1 viral particle budding. Are the GAG protein aggregates structurally sufficient to give rise to the observed cytoplasmic bud conformations? The techniques discussed in this article demonstrate that the 3-dimensional structures captured by cryo-EM tomography and confocal and fluorescence microscopy can be transformed into quantitative structural models that report forces and, potentially, the structural nature of cellular processes in vivo.

Methods

The measurements were performed by using a custom apparatus composed of 2 optical traps integrated with a fluorescence microscope. (See Fig. 4*A* for a schematic drawing of the vesicle force-extension apparatus.) Forces were applied to vesicles by binding streptavidin-coated 1-μm beads to DOPC giant unilamellar vesicles doped with biotin and TRITC. The vesicles were composed of 99% DOPC, 0.5% DOPE-biotin, and 0.5% DOPE-TRITC by molar fraction. The product numbers for the reagents used from Avanti Polar Lipids were: DOPC, 850375; DOPE-rhodamine, 810150; and DOPE-biotin, 870282. The beads used were Invitrogen catalog no. F-8777 FluoSpheres NeutrAvidin-labeled 1-μm nonfluorescent microspheres.

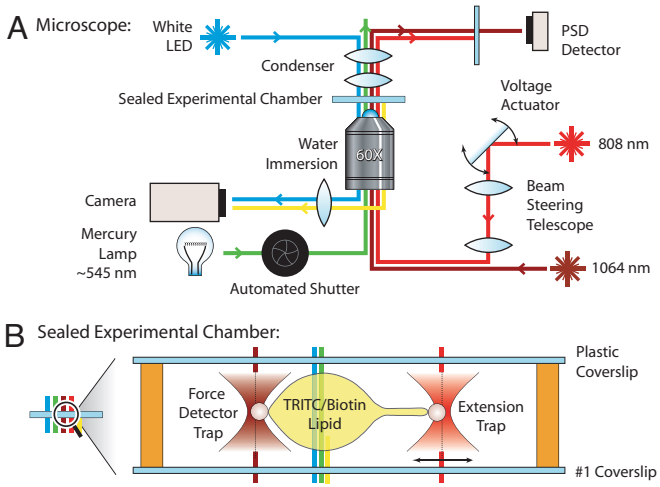

Fig. 4. Experimental apparatus schematic drawing. (*A*) The measurements were performed by using a custom setup composed of 2 optical traps integrated with a fluorescence microscope. The beam deflection from the 1,064-nm trap was detected in the back focal plane by a position sensitive detector (PSD). A second 808-nm trap with a beam-steering telescope was used to deform the vesicles. (*B*) Experimental chamber detail. The experiments were performed in a sealed 2-input flow chamber. Forces were applied to vesicles by binding streptavidin-coated 1-μm beads to DOPC giant unilamellar vesicles labeled with biotin and TRITC. Images of the fluorescently labeled lipid were analyzed to extract dynamic information about thermal membrane fluctuations and to calculate the static elastic forces.

A 1,064-nm trap was used as a force detector. The beam deflection was detected in the back focal plane by a position-sensitive detector (PSD) (42). A second 808-nm trap was used to deform the vesicles. This second color trap was used to avoid cross-talk between the deflection and force detection beams at the PSD. The position of the 808-nm trap was varied by using a beam-steering telescope driven by a computer-controlled voltage actuator.

The radius of a typical vesicle was $\approx$15 μm. To avoid membrane contact with the surface, experiments were performed at a distance of $\approx$100 μm from both surfaces of the experimental chamber. To trap beads at these long working distances, it was necessary to employ a 60$\times$ water-immersion objective. The trap stiffness was nearly independent of the working distance. The vesicles were imaged by using TRITC fluoresence, excited by a mercury lamp. Bead fishing was performed by using brightfield microscopy, lit by a white LED. Vesicles were imaged by using a Hamamatsu ORCA 285 camera.

The vesicle extensions were performed in a 2-input flow chamber. After blocking the chamber with BSA, the vesicle solution was pipetted into one of the input ports to fill the chamber. This input port was then sealed and the buffer was allowed to slowly evaporate from the unsealed input port, increasing the external osmotic pressure. When the vesicles became sufficiently soft, a charge of streptavidin-coated 1-μm beads was pipetted into the remaining input port and the port was sealed. The flow chamber is depicted schematically in Fig. 4*B*.

The diffusion constant of beads in the sucrose solution used in this experiment was measured by tracking the diffusion of 1-μm beads, with no lipid present, in the sealed 2-input flow chamber described above. A custom software package, kindly provided by Robert Bao, was used to analyze the time-series images of bead diffusion. The diffusion constant for water was measured to be 0.88 cP and that of the bead solution to be 0.98 cP. Measurement of piconewton forces with optical traps is a well-studied subject, reviewed, e.g., in Neuman and Block (43). Note that we have checked that the size of the fluctations (the spring constant) remains nearly constant during vesicle extension experiments implying that the presence of the vesicle does not affect the trap stiffness and the trap remains in the linear regime.

ACKNOWLEDGMENTS. We thank Robert Bao for the diffusion analysis code; Steve Quake for equipment generously loaned to us; Tristan Ursell, Lin Ma, Feng Feng, Sriram Subramaniam, and Grant Jensen for helpful discussions; and 2 anonymous reviewers for their contributions.

1. McMahon HT, Gallop JL (2005) Membrane curvature and mechanisms of dynamic cell membrane remodelling. *Nature* 438:590–596.
2. Frey TG, Mannella CA (2000) The internal structure of mitochondria. *Trends Biochem Sci* 25:319–324.
3. Ladinsky MS, Mastronarde DN, McIntosh JR, Howell KE, Staehelin LA (1999) Golgi structure in three dimensions: Functional insights from the normal rat kidney cell. *J Cell Biol* 144:1135–1149.
4. Sougrat R, *et al*. (2007) Electron tomography of the contact between t cells and siv/hiv-1: Implications for viral entry. *PLoS Pathog* 3:e63.
5. Cheng Y, Walz T (2007) Reconstructing the endocytotic machinery. *Methods Cell Biol* 79:463–487.
6. Gerlich D, Beaudouin J, Gebhard M, Ellenberg J, Eils R (2001) Four-dimensional imaging and quantitative reconstruction to analyse complex spatiotemporal processes in live cells. *Nat Cell Biol* 3:852–855.
7. Hess ST, *et al.* (2007) Dynamic clustered distribution of hemagglutinin resolved at 40 nm in living cell membranes discriminates between raft theories. *Proc Natl Acad Sci USA* 104:17370–17375.
8. Huang B, Wang W, Bates M, Zhuang X (2008) Three-dimensional super-resolution imaging by stochastic optical reconstruction microscopy. *Science* 319:810–813.
9. Fertuck HC, Salpeter MM (1974) Localization of acetylcholine receptor by ^{125}I-labeled alpha-bungarotoxin binding at mouse motor endplates. *Proc Natl Acad Sci USA* 71:1376–1378.
10. Unwin N (2005) Refined structure of the nicotinic acetylcholine receptor at 4a resolution. *J Mol Biol* 346:967–989.
11. Koster G, VanDuijn M, Hofs B, Dogterom M (2003) Membrane tube formation from giant vesicles by dynamic association of motor proteins. *Proc Natl Acad Sci USA* 100:15583–15588.
12. Rodriguez-Boulan E, Kreitzer G, Musch A (2005) Organization of vesicular trafficking in epithelia. *Nat Rev Mol Cell Biol* 6:233–247.
13. Vale RD, Hotani H (1988) Formation of membrane networks in vitro by kinesin-driven microtubule movement. *J Cell Biol* 107:2233–2241.
14. Waterman-Storer CM, Worthylake RA, Liu BP, Burridge K, Salmon ED (1999) Microtubule growth activates rac1 to promote lamellipodial protrusion in fibroblasts. *Nat Cell Biol* 1:45–50.
15. Sheetz MP (2001) Cell control by membrane-cytoskeleton adhesion. *Nat Rev Mol Cell Biol* 2:392–396.
16. Ledesma MD, Dotti CG (2003) Membrane and cytoskeleton dynamics during axonal elongation and stabilization. *Int Rev Cytol* 227:183–219.
17. Antonny B, Gounon P, Schekman R, Orci L (2003) Self-assembly of minimal copii cages. *EMBO Rep* 4:419–424.
18. Razani B, Lisanti MP (2001) Caveolins and caveolae: Molecular and functional relationships. *Exp Cell Res* 271:36–44.
19. Bruinsma R, Pincus P (1996) Protein aggregation in membranes. *Curr Opin Solid State Mater Sci* 1:401–406.
20. Reynwar BJ, *et al*. (2007) Aggregation and vesiculation of membrane proteins by curvature-mediated interactions. *Nature* 447:461–464.
21. Feng F, Klug WS (2006) Finite element modeling of lipid bilayer membranes. *J Comput Phys* 220:394–408.
22. Baumgart T, Hess ST, Webb WW (2003) Imaging coexisting fluid domains in biomembrane models coupling curvature and line tension. *Nature* 425:821–824.
23. Seifert U (1997) Configurations of fluid membranes and vesicles. *Adv Phys* 46:13–137.
24. Helfrich W (1973) Elastic properties of lipid bilayers: Theory and possible experiments. *Z Naturforsch* 28:693–703.
25. Canham PB (1970) The minimum energy of bending as a possible explanation of the biconcave shape of the human red blood cell. *J Theor Biol* 26:61–81.
26. Evans EA (1974) Bending resistance and chemically-induced moments in membrane bilayers. *Biophys J* 14:923–931.
27. Jenkins JT (1977) Static equilibrium configurations of a model red blood cell. *J Math Biol* 4:149–169.
28. Singer SJ, Nicolson GL (1972) The fluid mosaic model of the structure of cell membranes. *Science* 175:720–731.
29. Kusumi A, *et al*. (2005) Paradigm shift of the plasma membrane concept from the 2-dimensional continuum fluid to the partitioned fluid: High-speed single-molecule tracking of membrane molecules. *Annu Rev Biophys Biomol Struct* 34:351–378.
30. Capovilla R, Guven J (2004) Stress and geometry of lipid vesicles. *J Phys Condens Matter* 16:S2187–S2189.
31. Fygenson DK, Marko JF, Libchaber A (1997) Mechanics of microtubule-based membrane extension. *Phys Rev Lett* 79:4497–4500.
32. Cuvelier D, Derenyi I, Bassereau P, Nassoy P (2005) Coalescence of membrane tethers: Experiments, theory, and applications. *Biophys J* 88:2714–2726.
33. Rawicz W, Olbrich KC, McIntosh T, Needham D, Evans E (2000) Effect of chain length and unsaturation on elasticity of lipid bilayers. *Biophys J* 79:328–339.
34. Waugh RE, Hochmuth RM (1987) Mechanical equilibrium of thick, hollow, liquid membrane cylinders. *Biophys J* 52:391–400.
35. Waugh RE, Song J, Svetina S, Zeks B (1992) Local and nonlocal curvature elasticity in bilayer membranes by tether formation from lecithin vesicles. *Biophys J* 61:974–982.
36. Heinrich V, Bozic B, Svetina S, Zeks B (1999) Vesicle deformation by an axial load: from elongated shapes to tethered vesicles. *Biophys J* 76:2056–2071.
37. Powers TR, Huber G, Goldstein RE (2002) Fluid-membrane tethers: Minimal surfaces and elastic boundary layers. *Phys Rev E* 65:041901.
38. Baumgart T, Das S, Webb WW, Jenkins JT (2005) Membrane elasticity in giant vesicles with fluid phase coexistence. *Biophys J* 89:1067–1080.
39. Tian A, Johnson C, Wang W, Baumgart T (2007(Line tension at fluid membrane domain boundaries measured by micropipette aspiration. *Phys Rev Lett* 98:208102.
40. Upadhyaya A, Sheetz MP (2004) Tension in tubulovesicular networks of golgi and endoplasmic reticulum membranes. *Biophys J* 86:2923–2928.
41. Mills JP, Qie L, Dao M, Lim CT, Suresh S (2004) Nonlinear elastic and viscoelastic deformation of the human red blood cell with optical tweezers. *Mech Chem Biosyst* 1:169–180.
42. Visscher K, Gross SP, Block SM (1996) Construction of multiple-beam optical traps with nanometer-resolution position sensing. *IEEE J Select Top Quantum Electron* 2:1066–1076.
43. Neuman KC, Block SM (2004) Optical trapping. *Rev Sci Instrum* 75(9):2787–2809.